

Equation-free optimal switching policies for bistable reacting systems using coarse time-steppers.

Antonios Armaou*, Ioannis G. Kevrekidis†

November 20, 2018

Abstract

We present a computer-assisted approach to locating approximate coarse optimal switching policies between stationary states of chemically reacting systems described by microscopic/stochastic evolution rules. The “coarse time-stepper” constitutes a bridge between the underlying kinetic Monte Carlo simulation and traditional, continuum numerical optimization techniques formulated in discrete time. The approach is illustrated through two simple catalytic surface reaction models, implemented through kinetic Monte Carlo: *NO* reduction on *Pt*, and *CO* oxidation on *Pt*. The objective sought in both cases is to switch between two coexisting stable stationary states by minimal manipulation of a macroscopic system parameter.

keywords: equation-free, dynamic optimization, coarse timesteppers, kinetic Monte-Carlo, Hooke-Jeeves

1 Introduction

The computation of operating conditions that are optimal with respect to a predetermined objective (derived from economic considerations, safety requirements and product quality constraints) has been, for many decades, an exciting research area for chemically reacting systems. Increase in computational power has led to increased attention to dynamically evolving processes and the search for optimal time-varying operation protocols, both for lumped and spatially distributed systems (e.g., [47, 49, 1, 46, 3]). Interestingly, as sensing and actuation become increasingly more resolved in space and time for emerging chemical processes, spatiotemporally complicated operating policies can be considered (e.g., [50, 37, 19]). The problem of computing optimal transition paths over complicated free energy surfaces (see e.g., [9]) is also computationally related, especially considering Jarzynski’s relation between equilibrium free energy and nonequilibrium work (see e.g., [44]).

Existing computational approaches for solving dynamic optimization problems at the deterministic, continuum level may involve (a) formulation as a temporally discretized problem (both for the process and for the operating variable(s)) simultaneously, and solution using large sparse linear algebra techniques (e.g [48, 5, 47]); (b) formulations involving direct integration of the model equations in time, keeping track of possible constraint violations and temporal discretization of the operating variables [8, 10, 49, 2]; or possibly (c) using efficient solution algorithms within a dynamic programming formulation [29, 31, 4]. Knowledge of a macroscopic process model, in the form of macroscopic mass balances closed through appropriate constitutive expressions -such as chemical kinetic rate formulas-, is a fundamental prerequisite for these computational solution strategies.

In contemporary engineering applications, however, we are often faced with problems for which the available physical description is in the form of atomistic / stochastic evolution rules (e.g., kinetic Monte Carlo, Lattice Boltzmann, molecular dynamics, Brownian dynamics) while the design, optimization or control is required at a coarse-grained, macroscopic level. The lack of a closed-form process model can in principle be circumvented during the formulation of steady state optimization problems through the construction of identification algorithms “wrapped” around black box simulators (e.g., see [41]). Through design of computational experiments, sampling and estimation, one can determine the form of “surrogate” models that are subsequently used to identify local

*Department of Chemical Engineering, The Pennsylvania State University, State College, PA 16802, E-mail:armaou@enr.psu.edu

†Department of Chemical Engineering, PACM and Mathematics, Princeton University, Princeton, NJ 08544, E-mail:yannis@princeton.edu

or global (e.g., see [22, 35]) optima. In another approach, near optimal solutions are found for unconstrained optimization problems, under the assumption that absolute and relative error bounds are known for the computed objective function values [24].

Over the last few years we have been developing an *equation-free* computational approach enabling microscopic / stochastic simulators to *directly* perform system-level tasks, such as coarse integration, stability analysis, bifurcation/continuation and feedback control, thus circumventing the derivation of explicit macroscopic evolution equations [45, 14, 25, 40]. In this work we demonstrate the applicability of this computational enabling technology to coarse-grained optimization tasks; in particular, we present a formulation methodology capable of addressing dynamically evolving processes, to derive optimization formulations that can be solved employing standard, off-the-shelf direct search algorithms. The approach is applied to computationally identify coarse optimal operating parameter policies capable of switching the (expected) behavior of kinetic Monte Carlo simulators from one stationary state to another (alternatively, from the bottom of one potential well to the bottom of another); this is illustrated through kinetic Monte Carlo (KMC) simulations of two simplified models of heterogeneous catalytic chemical reactions. Both these systems are characterized by two “coarse-grained” stable stationary states. We seek optimal (for a particular definition of a cost function) parameter variation policies that will switch the KMC simulation from one stationary state to the other within a finite time interval.

The paper is organized as follows: In the following Section we present the problem we want to solve and our two illustrative examples. We then present our formulation for coarse-grained computational optimization. In the following two Sections we present detailed computational results for each of our illustrative problems; we then conclude with a brief discussion.

2 Process description

We investigate microscopic/stochastic processes for which we believe that the coarse-grained, expected dynamics can be well approximated in closed form by an equation of the general type

$$\dot{x} = F(x, p) \tag{1}$$

but where the right-hand-side of the evolution law, F , is not available in closed form. Here, $x(t) \in \mathbb{R}^n$ is a state variable vector, t is the time, \dot{x} is the time derivative of x , $\frac{dx}{dt}$, and $p \in \mathcal{P}^m$ is the vector of process parameters ($\mathcal{P}^m \subset \mathbb{R}^m$ is the subset of accessible values of the process parameters). The state variables $x(t)$ in the model of Eq.1 are coarse-grained observables of the microscopic simulation - typically a few lower order moments of an atomistically or stochastically evolving distribution (e.g., a concentration, or, in our heterogeneous catalytic reaction examples, a surface coverage, the zeroth moment of the distribution of adsorbates on the surface). The (unavailable) equation for the expected behavior of the process may possess, at fixed process parameter values, one or more steady states $x_{ss,i}$. We will assume that initially the microscopic process is in the neighborhood of one of these stable, coarse-grained stationary states, represented by $x_{ss,1}$ for the system of Eq.1.

2.1 The coarse time-stepper

The basis of our approach is the computation of a deterministic optimal policy - a time-dependent protocol for changing one of the operating parameters of the process- so as to attain a particular goal for the expected dynamics of the process (the “coarse-grained dynamics”): switching from one stationary state to another one. We want to accomplish this by acting directly on the microscopic simulator, thus circumventing the necessity of first deriving a closed form evolution equation for these coarse-grained dynamics. This deterministic policy for the coarse-grained behavior will then be applied to individual realizations of the process. As we will discuss below, it is convenient in our approach to reformulate the coarse dynamics in discrete rather than continuous time. The coarse-grained evolution law then takes the form:

$$x_{i+1} = G_T(x_i, p_{i+1}) \tag{2}$$

where t_i is the time at the beginning of i -th time interval, T is the time interval duration (reporting horizon), G_T represents the evolution of Eq.1 for constant process parameter value $p(t) = p_{i+1}$, $\forall t \in (t_i, t_i + T]$, initialized at x_i and evolved for time T , arriving at state x_{i+1} .

Conventional algorithms for the solution of optimization problems involving G_T incorporate frequent calls to a subroutine that *evaluates* G_T and/or the action of its derivatives in phase and parameter space on initial conditions. Equation-free based algorithms *estimate* the same quantities by short bursts of (possibly ensembles of) microscopic simulations *conditioned on* the same macroscopic initial conditions ([45, 14, 25, 40, 26]). The coarse time-stepper constitutes such an *estimate* of the discrete-time, macroscopic input-output map G_T obtained via the kinetic Monte Carlo simulator. Through a *lifting* operator the macroscopic initial condition is translated into several consistent microscopic initial conditions (distributions conditioned on a few of their lower moments). In some cases constructing microscopic initial conditions consistent with macroscopic observable quantities is easy (e.g., constructing distributions with prescribed means and variances); in other cases (e.g., when we want to prescribe pair probabilities on a lattice, or even a pair correlation function) an optimization problem may need to be solved to successfully lift; short runs with constrained dynamics algorithms ([39, 13, 12]) can also help in preparing such consistent microscopic initial conditions.

This ensemble of microscopic initial conditions is then evolved microscopically, in an easily parallelizable fashion (one consistent realization per CPU) for a relatively short time. The results are averaged through a *restriction* operator back to a macroscopic “output”; it is precisely this output that traditional algorithms simply compute through function evaluations when the evolution equations are available in closed form. As extensively discussed in [33, 25] part of the microscopic evolution is spent in a “healing” process - the higher moments, which have been initialized “wrong” quickly relax to functionals of the low order moments (our state variables). A separation of time scales (fast relaxation of the high moments to functionals of the low ones, and slow - deterministic- evolution of the low ones) underpins the existence of deterministic coarse grained evolution laws. The dynamics of the evolving microscopic distribution moments in the problems we study constitute thus a singularly perturbed system. The requirement of finite time microscopic evolution (necessary for the moment healing process) conforms with the discrete-time formulation of the coarse optimization problem, which is common in many optimization algorithms (see section 3 below).

2.2 Numerical experiments

We illustrate the proposed combination of traditional optimization techniques with stochastic simulators through KMC realizations (using the stochastic simulation algorithm, proposed by Gillespie [15, 16, 17]) of kinetic models describing catalytic NO reduction by H_2 and CO oxidation by O_2 , respectively.

We initially apply the proposed method to a drastically simplified kinetic model of NO reduction by H_2 on Pt surfaces; the model involves Langmuir adsorption, first order desorption, and chemical reaction requiring two neighboring vacant sites. The mean field Langmuir-Hinshelwood approximation of the kinetic mechanism we will model consists of a single Ordinary Differential Equation for the surface coverage of NO :

$$\frac{d\theta}{dt} = \alpha(1 - \theta) - \gamma\theta - k(1 - \theta)^2\theta. \quad (3)$$

Here θ describes the surface coverage of adsorbed NO , α , γ are the NO adsorption rate (incorporating the dependence of gas phase pressure of NO) and desorption rate constants respectively, and k is the reaction rate constant. The reaction term is third order due to the need for two free adjacent sites for the adsorption of H_2 . In Figure 2 we present the deterministic bifurcation diagram in the form of coverage θ_{ss} at steady-state as a function of k for $\alpha = 1$ and $\gamma = 0.01$. We observe a range of k values for which the system exhibits multiple steady-states; the higher and lower ones are locally stable, while the middle one is unstable.

The proposed approach is also applied to a kinetic Monte Carlo description of the CO oxidation reaction mechanism, using a simplified model for the reaction kinetics of the form $A + 1/2B_2 \rightarrow AB$. The kinetics here involve Langmuir adsorption for A , dissociative adsorption for B_2 , and a second order surface reaction whose products are immediately desorbed. The mean field approximation equations for this mechanism in the absence of adsorbate interactions would consist of a set of two ODEs [33]:

$$\begin{aligned} \frac{d\theta_A}{dt} &= \alpha(1 - \theta_A - \theta_B) - \gamma\theta_a - 4k_r\theta_A\theta_B \\ \frac{d\theta_B}{dt} &= 2\beta(1 - \theta_A - \theta_B)^2 - 4k_r\theta_A\theta_B \end{aligned} \quad (4)$$

where θ_A and θ_B describe the surface coverage of adsorbed CO and O_2 respectively, α and β denote the adsorption rate constants of CO and O_2 respectively, γ the desorption rate constant of CO , and with k_r we denote the

oxidation rate constant. In Figure 3 we present the deterministic bifurcation diagram representing the coverage of A, θ_A , and B, θ_B , respectively, as a function of the adsorption rate constant β for values of $\alpha = 1.6$, $\gamma = 0.04$ and $k_r = 1$. We observe that the system exhibits multiple steady states, the higher and lower ones being locally stable and the middle one unstable. Note that when the steady-state value of A coverage is low, then the coverage of B is high and vice-versa. A description of the use of the coarse KMC time-stepper in obtaining “coarse” versions of this bifurcation diagram may be found in [33].

3 Coarse computational optimization

Computing the temporal profiles of the process parameters that cause the transition of the coarse-grained system from one initial stationary state to a different final one can be formulated as an optimization problem; the objective is to minimize an integral cost function over time:

$$\min_{p(t) \in \mathcal{P}^m} \int_0^\infty \mathcal{Q}(t, x, p) dt \quad (5)$$

where \mathcal{Q} is a continuous scalar cost function. The constraints for this coarse optimization problem are the (unavailable) coarse process evolution equations Eq.1, the initialization at one of the coarse stationary states for $p = p_{ss}$, the requirement of termination at a different stationary state for the same process parameter value p_{ss} , as well as, possibly, other inequality constraints $g(x, p)$ (e.g., that surface coverages should remain positive and sum up to less than 1 at all times):

$$\begin{aligned} \dot{x} - F(x(t), p(t)) &= 0, & g(x, p) &\leq 0 \\ p(0) &= p_{ss}, & \lim_{t \rightarrow \infty} p(t) &= p_{ss} \\ x(0) &= x_{ss,1}, & \lim_{t \rightarrow \infty} x(t) &= x_{ss,2}. \end{aligned} \quad (6)$$

This constitutes an infinite dimensional problem in continuous time. Direct solution methods are based on the calculus of variations. Semi-infinite programming approaches provide us with the necessary mathematical tools to solve such problems with finite time horizon [20], through discretization of the temporal domain.

Another approach consists of approximating this problem through a finite time horizon problem with a final state penalty, which is (in our case) solved in discrete time. This results in a finite dimensional, generally nonlinear, optimization problem which -if the coarse equations are available- could be solved using available optimization techniques. For example, discretizing the process time $[0, t_f]$ in N time intervals of length T (not necessarily constant) and assuming that the process parameters remain constant within each interval, results in the following optimization program with $(N + 1) \times (n + m)$ variables and $n \times (N + 1) + m + n$ equality constraints:

$$\begin{aligned} \min_{p_i \in \mathcal{P}^m} \sum_{i=1}^N \int_{(i-1)T}^{iT} \mathcal{Q}_d(t, x_i, x_{i-1}, p_i) dt \\ + \mathcal{W}(R(|x(t_f) - x_{ss,2}| - \epsilon)) \\ \text{s.t.} \\ x_i = G_T(x_{i-1}, p_i) = 0, \quad i = 1, 2, \dots, N \\ g_d(x_0, \dots, x_N, p_0, \dots, p_N) \leq 0, \\ p_0 = p_{ss}, \quad x_0 = x_{ss,1}. \end{aligned} \quad (7)$$

Here \mathcal{Q}_d is analogous to the \mathcal{Q} function for the discrete values of the state, g_d is similarly analogous to g , $\mathcal{W}(\cdot)$ is a class K scalar function, $R(\cdot)$ is the ramp function and ϵ is a value for which $|x_N - x_{ss,2}| \leq \epsilon \iff \mathcal{W} = 0$. Appropriate final state penalty contributions to the objective function take the place of final state constraints at infinite time as stated in the original formulation of the problem; the final state is restricted to be (in finite time) within a neighborhood of the final stationary state. This fully discrete-time formulation is ideally suited for linking with a coarse time-stepper. It is also in principle possible to discretize only the process parameter temporal

behavior, resulting in the following formulation (coined *control vector parameterization* [48]) with $N \times m + 2n$ variables and n equality constraints:

$$\begin{aligned}
& \min_{p \in \mathcal{P}^m} \int_0^{t_f} \mathcal{Q}(t, x, p) dt \\
& \quad + \mathcal{W}(R(|x(t_f) - x_{ss,2}| - \epsilon)) \\
& \quad \text{s.t.} \\
& \quad \dot{x} - F(x, p) = 0, \quad g(x, p) \leq 0 \\
& \quad p(t) = \sum_{i=1}^N p_i \Pi\left(\frac{t}{T} - i + \frac{1}{2}\right) + p_{ss} H(-t)
\end{aligned} \tag{8}$$

where $\Pi(\cdot)$ is the standard boxcar function and $H(\cdot)$ denotes the Heaviside function. In cases where the explicit form of Eq.1 is unavailable, the state evolution is provided through direct simulation of the system.

3.1 Solution methodology

Traditional discrete time optimization schemes would repeatedly call, during the solution process, a numerical integration subroutine for the system equations (and possibly variational and sensitivity integrations for the estimation of derivatives with respect to state variables and parameters). This call is now substituted by the coarse time-stepper; the most important numerical issue is that of noise, inherent in the lifting process and the stochastic simulations, and the variance reduction necessary to estimate the state or its various derivatives. Simulations of different physical size systems (different lattice sizes in our simulation) are characterized by different values of variance. For the type of simulations in this paper, changing the physical size of the simulated domain on the one hand, and changing the number of copies of the simulation on the other, have comparable effects in reducing the variance of the simulation output; this, however, is not generally the case in KMC simulations. When a switching policy *for a particular physical size system* is required (e.g., for nanoscopic reacting systems, such as the chemical oscillations on Field Emitter tips [43]) variance reduction can be affected through a larger ensemble of consistent microscopic initializations (see also [34, 36] for variance reduction techniques). Simulation noise affects both function evaluations and (numerical) coarse derivative evaluations, and thus becomes an important element of the approach. It is interesting, however, to observe that massively parallel computation can reduce the *wall clock time* required for the computation distributing different microscopic initializations/realizations to different CPUs.

Due to the presence of noise in the coarse time-stepper results, the use of optimization algorithms that are specifically designed to be insensitive to noise becomes desirable and even necessary (the numerical estimation of derivatives is, of course, highly susceptible to noise). A class of search algorithms that fulfill this requirement are ones that use only function evaluations to search for the optimum, such as the Luus-Jaakola [32], Nelder-Mead and Hooke-Jeeves algorithms. Algorithms that use local and bounded approximations of the Jacobian matrix of the objective function with respect to the process parameters have also been developed, such as the implicit filtering algorithm; the reader may refer to [23, 27] for a review of these methods. In our approach, an optimization “wrapper” is constructed around an *on demand estimate* of the system coarse-grained model, constructed by computational experimentation with the microscopic solver. There is a close relation to the algorithms in [23, 27, 24], where comparable wrappers are constructed around *continuum* models that are difficult or expensive to evaluate (e.g., the ones that come from solutions of large PDEs). It is also remarkable that this “wrapper” approach, which performs the equation-free solution of an optimization problem through appropriate design of *computational* experiments, can be also in principle be used for the equation-free optimization of *experimental* systems. Indeed, if enough control authority exists for experiments to be initialized in detail, these optimization “wrappers” become protocols for the design of laboratory experiments leading to an optimum [18, 30, 38].

In all the above iterative algorithms [23], an appropriate initial guess of the process policy profile and a set of search directions for the $m \times N$ coarse-grained variables is required. The usual set of search directions (also used in our numerical experiment) is the unitary basis for $\mathbb{R}^{m \times N}$. Specifically for stencil-based search algorithms, important parameters also include a vector, the elements of which are the maximum distances the algorithm should venture from the current position during the new direction search step at each iteration. These perturbation distances are called *scales*.

Selection of these scales in the search algorithm requires estimates of noise bounds. A scale that is “too small” not only leads to increased computation time with no apparent advantages, but, especially in the case of algorithms that compute approximations of the Jacobian, can lead to grossly erroneous results for the search. The following time-stepper protocol yields, in our case, simulation results of bounded ensemble variance:

1. Initialize time-stepper. Set:
 - lattice size N_l ,
 - solution replica ensemble size M_r ,
 - minimum M_{min} and maximum M_{max} .
 - ensemble variance limit d_{max} and
2. In *each* time step, the time-stepper:
 - (a) simulates system for the desired parameter value M_r times (this can be affected through different microscopic initializations and/or different random seeds in the Monte Carlo process).
 - (b) Computes the standard deviation divided by the average of the sample, d .
 - (c) If $d > d_{max}$ and $M_r < M_{max}$, adjusts $M_r \geq M_{min}$, repeat step (a).

Adaptively adjusting the number of realization in the ensemble can thus help in the choice of appropriate scales. The lattice size N_l of the time-stepper routine affects the expected evolution of the process observables; for the SSA simulations in this paper, as the size of the simulation increases the expected behavior of the stochastic microscopic process becomes closer and closer approximated by the mean-field description represented by the ODE system [16]. In our computations in this paper, the lattice size of our time-stepper is chosen so that the discrepancy between the expected behavior obtained from the KMC simulations and the ODE solutions is negligible [11]; this way we can validate the directly computed optimal switching policies by comparing them to the mean-field, deterministic ones. Changing the lattice size will, in general, affect the expected behavior of a stochastic process; the variance of the time-stepper results will also be affected. We will use multiple replica simulation runs M_r (with the same process settings and macroscopic initial conditions) to control fluctuations in the estimation of the expected results.

3.2 Direct search method: The Hooke-Jeeves algorithm

The processes that we investigate often lead to optimization problems, where the objective functions exhibit a large number of small local optima that in effect “hide” the directions along which the objective function decreases. This is due to the stochastic nature of the microscale simulations that are used to infer the dynamic behavior of the coarse variables.

A class of search algorithms that avails itself to the solution of such problems is direct search algorithms. These methods evaluate the objective function at sample points and use the provided information to continue sampling along promising directions. A prerequisite is an initial point inside the feasible region as well as a set of search directions. A number of such methods exist including Nelder-Mead, Hooke-Jeeves, Multi-Coordinate Search (MCS); in the current work we use the Hooke-Jeeves method. For completeness we briefly describe the method (the reader is referred to [23] for a detailed presentation).

Hooke-Jeeves is a stencil based method, similar to coordinate descent; however it is a more aggressive search. As in all stencil-based methods, a set of search directions \mathbf{v} is provided, as well as an array of M scales, \mathbf{s} , that determine the step length size which the search algorithm is allowed to venture away from the current point when investigating for promising search directions. Let us define the design variable vector as $x \in \mathbb{R}^N$, the objective function as $f(\cdot)$, and (without loss of generality) the optimization problem as one of minimizing the objective function. In the following pseudocode we present the Hooke-Jeeves method, comprising of the following steps [23]:

- Define: Initial position, x_0 , search directions, \mathbf{v} , and scales, \mathbf{s} .
- search:
 1. Compute $f(x_0)$.

2. choose scale s_i from \mathbf{s} .
 3. Exploratory step:
 - 3.1 Define $x_s = x_0$.
 - 3.2 Investigate search direction $v_j \in \mathbf{v}$:
 - Compute $f(x_s + s_i v_j)$. If $f(x_s + s_i v_j) < f(x_0)$ define $x_s = x_s + s_i v_j$, move to step 3.3
 - If $f(x_s + s_i v_j) \geq f(x_0)$ compute $f(x_0 - s_i v_j)$.
 - If $f(x_s - s_i v_j) < f(x_0)$ define $x_s = x_s - s_i v_j$, continue to step 3.3.
 - 3.3 Repeat step 3.2 for $j = j + 1$. If $j = N$ (all N search directions in \mathbf{v} investigated) continue to step 3.4.
 - 3.4 Obtain promising direction $d_i = x_s - x_0$.
 4. If $d_i = 0$, then $i = i + 1$ (reduce scale size to s_{i+1}). If $i = M$ (all M scales in \mathbf{s} investigated) terminate search iterations.
 5. Pattern move step:
 - Define $x_c = x_0 + 2d_i$. Compute $f(x_c)$.
 - If $f(x_c) < f(x_s)$, set $x_s = x_c$.
 6. Set $x_0 = x_s$, and repeat step 1.
- Optimal point, x_0 , obtained.

In Figure 1 we sketch the application of the above pseudocode in a representative optimization problem with $N = 2$; only one iteration is presented. The optimal location in Figure 1 is represented by x_{opt} , and darker contour lines present decreasing values of the objective function. Position x_0 is chosen to initialize the search (step 1), and during the exploratory step (step 3), the objective function is evaluated in the search directions v_1 and v_2 and at a distance s_1 from x_0 . Two directions are computed to lead to lower objective function values (shown with arrows, step 3.2), thus defining x_s at the end of step 3.3 to be at the upper right, and proposing the move direction shown with the dotted arrow in Figure 1. During the pattern move step (step 5), an aggressive move to x_c is proposed (shown in Figure 1), and $f(x_c)$ is computed to be less than $f(x_s)$. As a result, the next iteration takes place at position x_c , shown in Figure 1

The method can be easily modified to incorporate inequality constraints for the variables x , by modifying the objective function to increase when x moves outside a feasible set. The search algorithm behavior at the boundaries is reminiscent of interior point methods. Optimization algorithms that are based only on function evaluations are not guaranteed to converge to a global minimum, or even to a minimum. This is due to the fact that the necessary optimality conditions in the neighborhood of the result are *not computed*, and also because a search direction may have been neglected.

Once the optimization algorithm has converged and produced an “apparent best” operating policy profile, it may be prudent to restart using the result of the previous search as an initial guess. Restarting the search, which invokes again the “large” scales, will cause large perturbations in the operating policy profile, which may assist in finding a better local optimum. Once two consecutive runs have produced comparable results, the free variable profile is declared “optimal over all scales” [23]. We note that due to the use of KMC simulations, two simulation runs will not produce the same value of the objective function for the *same* policy. This results in small variations of the identified policy profiles in two consecutive searches, if small scales are used (scales that lead to perturbations in the system state evolution that are comparable to the noise of the KMC simulations).

4 Numerical Results: NO reduction on Pt surface

The approach outlined in section 3.1 was initially applied towards the computation of an optimal switching policy (between different stationary states) in our simplified *NO* reduction model. We define a (slightly arbitrary, but useful for illustration purposes) objective function in Eq.8 as:

$$\mathcal{Q} = (k(t) - k_{ss})^2 (1 - 0.3e^{-t}) T \left(\sum_{i=0}^N \delta(t - iT) \right)$$

$$\mathcal{W} = 50 [1 - \exp(-R(|\theta(t_N) - \theta_{ss,f}| - \epsilon))]$$

where $\epsilon = 0.05$, R denotes the ramp function and δ denotes the standard Dirac function. We assume that the single “manipulated variable” for this problem (the process parameter p of Eq.1) is the (macroscopic) reaction rate constant k ; this affects the reaction probability in the microscopic simulation. In continuum models the reaction rate constant could be manipulated, for example, by changes in temperature, through its Arrhenius temperature dependence; our adsorption rate constants could be varied by changes in the gas phase pressure of a species. The options that were used for the specific optimization problem are presented in Table 1. The form of \mathcal{Q} reflects the formulation of the time-dependent policy through a finite number of decisions, placing a penalty at the time of decision. \mathcal{W} is a class K function penalizing the deviation of the final state from the desired steady-state heavily initially, reaching a plateau at the maximum deviation of θ .

KMC simulations based on the Gillespie SSA algorithm formed the basis of the coarse time-stepper that was used to estimate the coarse-grained system response. A variety of lattice and sample sizes were used in estimating the dynamic behavior of the system. Hooke-Jeeves was the algorithm of choice in our search for the optimal profile. In Table 2 we present the value of the objective function for the computed optimal parameter profiles, through which the effect of the error in the computed optimal profile is implicitly quantified. The lattice size N_l was increased with no appreciable change in the expected system response.

A secondary gain from the lattice size increase was that the ensemble variance d decreased, since $d \propto (N_l)^{-1/2}$. Moreover, as the sample size M_r used to compute the coarse response increased in the KMC simulations, the ensemble variance d also decreased, as expected, since $d \propto (M_r)^{-1/2}$. This in turn lead to results from the search for the optimal profile of k that are closer to ones obtained when we use the time-stepper of the actual deterministic problem (for comparison purposes). The Gillespie stochastic simulation algorithm [15, 17] was chosen so that the coarse behavior at large sample sizes can be well approximated through deterministic ODEs, and so that the noisy time-stepper optimization results can be compared to the deterministic ones at the appropriate limit. The objective value convergence to the computed optimal value from the ODE “direct simulator” comes, of course, at the cost of increased computational work. This is only an illustrative example, to validate the approach; it would not make sense to use coarse-grained computations when good deterministic equations for the macroscopic behavior are known. The equation-free approach is intended for cases where the macroscopic equations are *not* available in closed form. The use of parallel computing can, as we discussed, drastically decrease the necessary wall-clock simulation time. In Figure 4 we present the results for $N_l = 500 \times 500$ and $M_r = 1000$ and compare them to the direct macroscopic ODE simulation results. A *near*-optimal parameter profile is arrived at, due to the combination of KMC simulations’ noise and the Hooke-Jeeves search algorithm (a search direction that has been investigated and characterized as unfavorable is not reinvestigated to conserve CPU time).

We also used an alternative algorithm (Implicit Filtering, [23]) to compute a near optimal steady state switching profile of $k(t)$. The method of implicit filtering uses consecutive bounded approximations of the Jacobian employing a set (varying at each iteration) perturbation of the design variables and poses a prescribed limit to the maximum change of the design variable at each iteration. The time-stepper protocol used had $d_{max} = 0.005$, with variable lattice size set at $N_l = 126 \times 126$ and $N_{max} = 4N_l$. Adaptively adjusting M_r , originally set at $M_r = 252$, with $M_{max} = 4M_r$ and $M_{min} = 0.5M_r$, the bounds on the ensemble variance were satisfied. We also note that a minimum lattice size bound was always enforced in order to ascertain that the discrepancy between the expectation of the finite-size KMC simulations and the mean-field ODEs for the same mechanism is negligible over the time scales we are working.

The resulting near optimal time profile of $k(t)$ is presented in Figure 5a, while the near optimal path of NO coverage evolution $\theta(t)$ is shown in Figure 5b for an averaged realization, and in Figure 5c for a single KMC realization with lattice size $N_l = 100 \times 100$ and reporting horizon $\delta t = 0.0039$.

In Table 3 we present computational results obtained through incorporating the coarse time-stepper in an implicit filtering algorithm. As one might expect, as the variance limit is decreased the algorithm -for a large enough lattice- approaches the optimal profile of $k(t)$ computed directly through the coarse ODE model. We also observe that a successful scales selection depends heavily on d_{max} , as scales below a certain limit have an adverse effect on the computed near optimal path result (compare the results of the search when the lowest scale is 2^{-4} to the one when it is 2^{-3}).

The time-stepper protocol can be combined with the search algorithm to solve the optimization program using successively more refined scales. A first search, with large values for the scales, can take place at higher d_{max} , followed by searches with gradually lower d_{max} and smaller scales to refine the search for the optimal path; this approach may lead to computational savings. When using the KMC with $d_{max} = 0.005$ and a lower scale of 2^{-3} for an initial search, followed by a KMC simulation of the system with $d_{max} = 0.0005$ and lower scale of 2^{-5} , we

find a near optimal path with $v = 10.4110$ in a total time of 3981 s. A search using KMC with $d_{max} = 0.001$ and lower scale of 2^{-4} lead to computing a near optimal path of $v = 10.4129$ in 6858 s (results are shown in Table 3).

The “optimal” switching path, shown in figure 5b, takes the (expected) phase point from $\theta_{ss,s}$ through the unstable steady state $\theta_{ss,i}$ as shown in Figure 5b. After this is accomplished, we observe that the optimal $k(t)$ trajectory rapidly converges back to k_{ss} (see Figure 5a). The coarse phase point is now within the region of attraction of the steady state $\theta_{ss,f}$, and no particular switching action is needed to get it there.

The objective function values presented in this section were computed, for comparison purposes, by integrating the coarse system Eq.3 for the optimal switching profile found. During the optimal search using KMC simulations, the coarse process model was *never* used. Several optimization algorithms were explored in conjunction with the coarse time-stepper, including Hooke-Jeeves, Nelder-Mead, Implicit-Filtering as well as Multilevel Coordinate Search (MCS). Hooke-Jeeves was primarily chosen due to the simplicity of the method and its relative convergence speed. Implicit Filtering algorithm was mainly used with the coarse time-stepper to illustrate the variance-reduction protocol. Enforcing an upper bound on the variance of the ensemble, along with the selection of the value of the scales, provided an order of magnitude estimate of the error in the estimated derivatives during the Jacobian approximation; variance reduction techniques may also be useful for this purpose.

5 Numerical Results: catalytic CO oxidation

After solving a one-dimensional (coarse grained) example, we used the same computational approach to find optimal switching policies between different stationary states of a simplified *CO* oxidation model presented in section 2.2. The (again slightly arbitrary, illustrative) objective function in Eq.8 was defined as:

$$\mathcal{Q} = (\beta(t) - \beta_{ss})^2 (1 - 0.3e^{-t}) T \left(\sum_{i=0}^N \delta(t - iT) \right)$$

$$\mathcal{W} = 50 [1 - \exp(-R(|\theta_{CO}(t_N) - \theta_{CO,ss,f}| - \epsilon) - R(|\theta_{O_2}(t_N) - \theta_{O_2,ss,f}| - \epsilon))]]$$

where $\epsilon = 0.05$, R denotes the ramp function and δ denotes the Dirac function. The single “manipulated variable” for this problem (the process parameter p of Eq.1) was chosen to be the oxygen O_2 adsorption rate constant β , which can in principle be manipulated experimentally by varying the oxygen gas phase pressure. The options that were used for the specific optimization problem are presented in Table 4. In figure 6 we present the phase portrait of the system under the specific nominal process parameter settings. The evolving coarse-grained system has to traverse a one-dimensional separatrix in two phase-space dimensions, in order to enter the basin of attraction of the desired *CO* rich steady-state.

The kinetic Monte-Carlo time-stepper and the Hooke-Jeeves algorithm were used to compute the coarse optimal temporal profile of the O_2 adsorption rate $\beta(t)$ for large timesteps of $T = 0.5$ and lattice size of 100×100 and averaging of 200 runs to describe the process evolution. For comparison purposes the optimal profile was also identified, using successive quadratic programming (SQP), when the constraints were computed through the integration of the mean field deterministic process model of Eq.4 (called the deterministic profile and program, respectively, for the rest of the section). The identified temporal profile of β is shown in Figure 7a with a blue line and is compared to the computed profile of the deterministic program, shown with a green line. The value of the objective function is $v_{MC,100 \times 100, 200} = 25.7498$, a relative error of 0.55% over the optimal value of $v_{LC} = 25.6096$. The total time for the computation of the optimal profile using KMC (first initial run) was 8 minutes and 16 seconds. Note that the values of the objective presented -for comparison purposes, and only upon convergence- are computed by applying the located optimal policy to the mean field ODE model of Eq.4. Similar results were also reached when using the deterministic mean field equations Eq.4 with Nelder-Mead after three search initializations and Hooke-Jeeves also after three search initializations. Presenting the *CO* and O_2 coverage in Figures 7c and 7d respectively, we observe that the *CO* oxidation evolves similarly for both β profiles and both realizations (the deterministic and the KMC-based one). The same observation is made in Figure 7b, the phase portrait of the process evolution. We observe that the two evolution profiles, the coarse-grained one using the KMC computed optimal policy (green line) and the one computed by integrating Eq.4 lie close to each other at all times.

To obtain a better resolved approximation of the continuous-time optimal manipulation of parameter β , we decreased the time-step to $T = 0.1$. The discrete-time formulation was subsequently solved using the Hooke-Jeeves

algorithm; results are shown in Table 5. Specifically, the search algorithm was reinitialized three times, using the previously estimated optimal profile to initialize the search, before an optimal over all scales was declared in the case of the noise-free legacy simulator. Similarly, when using the KMC realization of the process, the search was terminated when the resulting optimal profile was a slight perturbation to the previous result and the average value of the objective (over ten simulations) was within error bounds of the previous value.

Initially, to solve the optimization problem of Eq.8 with the Hooke-Jeeves search algorithm we used a KMC realization of the process with a $N_l = 100 \times 100$ and $M_r = 200$ for the coarse time-stepper output; this combination identified the β temporal profile presented in Figure 8a (green line). We observe that the profile is a perturbation around to the resulting β profile (blue line) of the deterministic SQP search.

In Figure 8b we present the phase portrait of the process evolution for the coarse KMC-based HJ computed profile (blue line); the system response is closely related to the system behavior under the deterministic, SQP-computed, profile (green line). The same observation is also made based on the evolution of CO and O_2 coverage, shown in Figures 8c and 8d respectively. The closeness of the two phase portraits under the two different switching policies suggests that the objective function is relatively insensitive to the change of β , a further difficulty towards the computation of a truly optimal policy.

To better illustrate the effect of noise originating from the stochastic nature on the time stepper, we run ten independent KMC simulations with $N_l = 100 \times 100$, $M_r = 200$ for the switching policy of Figure 8. The average value of the objective function for these ten runs was $v_{av,MC} = 25.1272$ with standard deviation $\sigma_{MC} = 0.0241$, while the value given by the mean-field ODE model is given at Table 5, 1st line. Based on the intuition gained from these runs, we subsequently repeated the third pass of the specific search ten times. The objective function was then independently computed for the *previously* identified optimal profiles using the ODE model (for comparison purposes); the average value was computed to be $v_{av,LC} = 25.1928$ with standard deviation $\sigma_{LC} = 0.0681$. Let us reiterate that the KMC coarse time-stepper and the ODE time-stepper represent *different* approximate realizations of the same process and as such the predictions of the two time-steppers may lie very close, but in general they are not necessarily the same.

The increase in accuracy comes at a high computational cost, as can be seen from the total CPU time needed for each search, when using a KMC realization of the process with a 100×100 lattice size and an average of 200 runs, compared to when using a KMC realization of the process with a 300×300 lattice size and an average of 600 runs. In order to reduce the total computational cost, during the last run (line 3 in Table 5), we initially started a search with the accuracy of the coarse timestepper implicitly set at a low value (KMC realization with 100×100 lattice size and an average of 200 runs). Once the search converged, we indirectly increased the accuracy of the timestepper (KMC realization with 300×300 lattice size and an average of 600 runs) and initiated a second pass. The computational savings amounted to approximately 55000 seconds. Computational costs can be further reduced by adjusting the scales during each new search, taking into account the variance of the coarse time-stepper results ensemble. Using a KMC realization of the process with a 300×300 lattice size and an average of 600 runs for the coarse time-stepper output, the Hooke-Jeeves search algorithm identified the β temporal profile presented in Figure 9a (green line). This compares well with the β profile (blue line) resulting from a deterministic SQP search.

Furthermore, in Figure 9b we present the phase portrait of the process evolution for the coarse-KMC based, HJ computed profile (blue line) and the deterministic SQP-computed profile (green line); we observe that the system response is practically the same for both computed profiles of $\beta(t)$. The same observation is also made based on the evolution of CO and O_2 coverage, shown in Figures 9c and 9d respectively, for an averaged realization of the system, and in Figures 10a and 10b respectively for a single KMC realization, with time-step $\delta t = 0.0031$.

The located optimal system trajectory is also shown in Figure 11a for $T = 0.5$ and Figure 11b for $T = 0.1$, with a red line; the blue line represents the separatrix of the system (if it exists) for the current $\beta(t)$. The optimal switching policy takes the (expected) phase point from $\theta_{ss,s}$ through the separatrix of the saddle (unstable) steady state $\theta_{ss,i}$; note that during traversing the separatrix line of $\beta_s s$, $\beta(t)$ is reduced to a value where no unstable steady state (and thus separatrix) exists. After this is accomplished, the optimal $\beta(t)$ rapidly converges back to β_{ss} (see Figure 5a). The coarse phase point is now within the region of attraction of the steady state $\theta_{ss,f}$, and no particular action is needed.

Another way to accelerate the computation of the optimal switching policy, is by solving a sequence of optimization programs, reducing the time-step in each iteration from an initial “coarse” to a final “finer” one. In effect the suggestion is to use a method inspired from multigrid optimization methods (e.g., [6, 7]). During each iteration, we utilize the result of the previous iteration as an initial guess, which we adapt to the larger

number of decisions in time that we need to take. Specifically for this work, we used cubic splines to fit the optimal parameter profiles obtained from n -th iteration, and resampled in the new temporal domain to obtain the initial guess for the refined search of the $n + 1$ th iteration. Subsequently, during the $n + 1$ th iteration we use an off-the-shelf search algorithm to obtain optimal process parameter profiles. As is expected in all multigrid methods, the accuracy of the off-the-shelf search algorithm used has to be increased to converge closer to the optimal solution. This is done in our case by gradually reducing the size of the scales. Once we have reached the “finer” time-step and obtained the final solution using this method, one must investigate if the solution is “optimal over all scales”. This is accomplished in our case by performing a new search using scales with a wide range of values. In Table 6 we present the computational efforts needed, following the aforementioned procedure, using HJ algorithm with a 100×100 lattice with 200 run averaging, KMC realization of the process. In this case the scales were kept constant. We observe that we obtain a first pass of the HJ algorithm at $T = 0.1$ in a total of 3983 seconds.

6 Conclusions

We presented a computational methodology for the location of coarse-grained optimal operating parameter policies for chemically reacting systems described by microscopic/stochastic evolution rules. In particular, we approximated optimal operating policies switching bistable reacting systems from one stationary state to another; our approach is intended for systems for which macroscopic, coarse evolution equations exist but are not available in closed form. The advantage of the proposed method lies in the establishment, through the coarse time-stepper, of a computational bridge between atomistic/ stochastic simulators and traditional (in particular, derivative free) optimization algorithms. The approach can be directly extended to systems with higher dimensional expected behavior (see for example [33]), and possibly, through matrix-free methods, to systems with infinite dimensional (spatially distributed, but dissipative) expected behavior [14]. Current efforts are focused on applying this methodology to the study of coarse-grained optimal paths associated with transitions and rare events in computational chemistry; in this case the coarse timestepper will be estimated from processing the results of an “inner” molecular dynamics or an “inner” Monte Carlo simulator ([21, 28]). In this case, the knowledge of appropriate macroscopic observables (reaction coordinates) is crucial, and data processing techniques capable of extracting such reduced data descriptions (e.g., [42]) become important. The approach we described in this paper can be easily combined with “empirical” observables suggested by such data processing algorithms.

Acknowledgements

Financial support from the Air Force Office of Scientific Research (Dynamics and Control), National Science Foundation, ITR, and Pennsylvania State University, Chemical Engineering department, is gratefully acknowledged. The authors are indebted to professor Alexei G. Makeev of Moscow State University, department of Computational Mathematics and Cybernetics for providing the kinetic Monte Carlo time-steppers used in this work and Ee-Sunn Chia for the visualization of the CO oxidation trajectories.

References

- [1] A. Armaou and P. D. Christofides. Optimization of dynamic transport-reaction systems using nonlinear model reduction. *Chem. Eng. Sci.*, 57:5083–5114, 2002.
- [2] E. Balsa-Canto, J. R. Banga, A. A. Alonso, and V. S. Vassiliadis. Efficient optimal control of bioprocesses using second-order information. *Ind. Eng. Chem. Res.*, 39:4287–4295, 2000.
- [3] E. Balsa-Canto, J. R. Banga, A. A. Alonso, and V. S. Vassiliadis. Dynamic optimization of distributed parameter systems using second-order directional derivatives. *Ind. Eng. Chem. Res.*, 43:6756–6765, 2004.
- [4] D. P. Bertsekas. *Dynamic Programming: Deterministic and Stochastic Models*. Prentice Hall, Englewood Cliffs, NJ, USA, 1987.

- [5] L. T. Biegler, A. M. Cervantes, and A. Wächter. Advances in simultaneous strategies for dynamic process optimization. *Chem. Eng. Sci.*, 57:575–593, 2002.
- [6] T. Binder, L. Blank, W. Dahmen, and W. Marquardt. Iterative algorithms for multiscale state estimation.1. concepts. *J. Optim. Theory & Appl.*, 111:501–527, 2001.
- [7] T. Binder, L. Blank, W. Dahmen, and W. Marquardt. Iterative algorithms for multiscale state estimation. 2. numerical investigations. *J. Optim. Theory & Appl.*, 111:529–551, 2001.
- [8] T. Binder, A. Cruse, C. A. C. Villar, and W. Marquardt. Dynamic optimization using a wavelet based adaptive control vector parameterization strategy. *Comput. Chem. Eng.*, 24:1201–1207, 2000.
- [9] P. G. Bolhuis, D. Chandler, C. Dellago, and P. L. Geissler. Transition path sampling. Throwing ropes over rough mountain passes in the dark. *Annu. Rev. Phys. Chem.*, 53:291–318, 2002.
- [10] W. F. Feehery and P. I. Barton. Dynamic optimization with equality path constraints. *Ind. Eng. Chem. Res.*, 38:2350–2363, 1999.
- [11] K. A. Fichthorn and W. H. Weinberg. Theoretical foundations of dynamical Monte Carlo simulations. *J. Chem. Phys.*, 95:1090–1096, 1991.
- [12] C. W. Gear, T. Kaper, I. G. Kevrekidis, and A. Zagaris. Projecting to a slow manifold: Singularly perturbed systems and legacy codes. *SIAM J. Dyn. Sys.*, submitted, 2004.
- [13] C. W. Gear and I. G. Kevrekidis. Constraint-defined manifolds: a legacy-code approach to low-dimensional computation, in press. *J. Sci. Comp.*, 2004. also available as physics/0312094 @ arXiv.org.
- [14] C. W. Gear, I. G. Kevrekidis, and C. Theodoropoulos. “coarse” integration/bifurcation analysis via microscopic simulators: micro-Galerkin methods. *Comp. Chem. Engng.*, 26:941–963, 2002.
- [15] D. T. Gillespie. A general method for numerically simulating the stochastic time evolution of coupled chemical reactions. *J. Comp. Phys.*, 22:403–434, 1976.
- [16] D. T. Gillespie. Exact stochastic simulation of coupled chemical reactions. *J. Phys. Chem.*, 81:2340–2361, 1977.
- [17] D. T. Gillespie. A rigorous derivation of the chemical master equation. *Physica A*, 188:404–425, 1992.
- [18] P. A. Gilmore, S. S. Berger, R.F. Burr, and J. A. Burns. Automated optimization techniques for phase change piezoelectric ink jet performance enhancement. In *International Conference on Digital Printing Technologies, Society for Imaging Science and Technology, IST&T’s NIP 13*, pages 716–721, November 1997.
- [19] D. G. Grier. A revolution in optical manipulation. *Nature*, 424:810–816, 2003.
- [20] R. Hettich and K. O. Kortanek. Semi-infinite programming: Theory, methods, and applications. *SIAM Review*, 35:380–429, 1993.
- [21] G. Hummer and I.G.Kevrekidis. Coarse molecular dynamics of a peptide fragment: free energy, kinetics and long time dynamics computations, submitted. *J. Chem. Phys.*, 2002.
- [22] D. R. Jones, M. Schonlau, and W. J. Welch. Efficient global optimization of expensive black-box functions. *J. Global Opt.*, 13:455–492, 1998.
- [23] C. T. Kelley. *Iterative Methods for Optimization*, volume 18 of *Frontiers in Applied Mathematics*. SIAM, Philadelphia, PA, USA, 1999.
- [24] C. T. Kelley and E. W. Sachs. Truncated newton methods for optimization with inaccurate functions and gradients. *JOTA*, 116:83–98, 2003.
- [25] I. G. Kevrekidis, C. W. Gear, J. M. Hyman, P. G. Kevrekidis, O. Runborg, and K. Theodoropoulos. Equation-free multiscale computation: enabling microscopic simulators to perform system-level tasks, submitted. *Comm. Math. Sciences*, 2002. Also available as physics/0209043 at arXiv.org.

- [26] I. G. Kevrekidis, C. William Gear, and G. Hummer. Equation-free: the computer-assisted analysis of complex, multiscale systems. *AIChE J.*, 50:1346–1354, 2004.
- [27] T. G. Kolda, R. M. Lewis, and V. Torczon. Optimization by direct search: New perspectives on some classical and modern methods. *SIAM Review*, 45:385–482, 2003.
- [28] D. I. Kopelevich, A. Z. Panagiotopoulos, and I. G. Kevrekidis. Coarse-grained kinetic computation of rare events: application to micelle formation. *J. Chem. Phys.*, submitted, 2004. Also found at [arXiv.org/cond-mat/0407219](https://arxiv.org/cond-mat/0407219).
- [29] D. Kossman and K. Stocker. Iterative dynamic programming: A new class of query optimization algorithms. *ACM Trans. Dat. Sys.*, 25:43–82, 2000.
- [30] R. J. Levis, G. M. Menkir, and H. Rabitz. Selective bond dissociation and rearrangement with optimally tailored, strong-field laser pulses. *Science*, 292:709–713, 2001.
- [31] R. Luus. *Iterative Dynamic Programming*. Chapman & Hall/CRC, London, UK, 2000.
- [32] R. Luus and T. H. I. Jaakola. Optimization by direct search and systematic reduction of the size of search region. *AIChE J.*, 19:760–766, 1973.
- [33] A. G. Makeev, D. Maroudas, and Kevrekidis I. G. “Coarse” stability and bifurcation analysis using stochastic simulators: Kinetic Monte Carlo examples. *J. Chem. Phys.*, 116:10083–10091, 2002.
- [34] M. Melchior and H. C. Oettinger. Variance reduced simulations of stochastic differential equations. *J. Chem. Phys.*, 103:9506–9509, 1995.
- [35] C. A. Meyer, C. A. Floudas, and A. Neumaier. Global optimization with nonfactorable constraints. *Ind. Eng. Chem. Res.*, 41:6413–6424, 2002.
- [36] H. C. Oettinger. *Stochastic Processes in Polymeric Fluids*. Springer Verlag, Berlin-Heidelberg, 1996.
- [37] A. G. Papatheanasiou, J. Wolff, I. G. Kevrekidis, H. H. Rotermund, and G. Ertl. Some twists and turns in the path of improving surface activity. *Chem. Phys. Lett.*, 358:407–412, 2002.
- [38] H. A. Rabitz, M. M. Hsieh, and C. M. Rosenthal. Quantum optimally controlled transition landscapes. *Science*, 303:1998–2001, 2004.
- [39] J. P. Ryckaert, G. Ciccotti, and H. Berendsen. Numerical integration of the cartesian equations of motion of a system with constraints: molecular dynamics of N-alkanes. *J. Comp. Phys.*, 23:327, 1977.
- [40] C. I. Siettos, A. Armaou, A. G. Makeev, and I. G. Kevrekidis. Microscopic/stochastic timesteppers and coarse control: a kinetic Monte Carlo example, accepted. *AIChE J.*, 49:1922–1926, 2003.
- [41] C. I. Siettos, C. C. Pantelides, and I. G. Kevrekidis. Enabling dynamic process simulators to perform alternative tasks: A time-stepper based toolkit for computer-aided analysis. *Ind. Eng. Chem. Res.*, 42:6795–6801, 2003.
- [42] A. J. Smola, O. L. Mangasarian, and B. Schoelkopf. Sparse kernel feature analysis. Data Mining Institute Technical Report 99-04, University of Wisconsin Madison, 1999.
- [43] Yu. Suchorski, J. Beben, E. W. James, J. W. Evans, and R. Imbihl. Fluctuation-induced transitions in a bistable surface reaction: Catalytic CO oxidation on a Pt field emitter tip. *Phys. Rev. Lett.*, 82:1907, 1999.
- [44] S. X. Sun. Equilibrium free energies from path sampling of nonequilibrium trajectories. *J. Chem. Phys.*, 118:5769–5775, 2003.
- [45] K. Theodoropoulos, Y.-H. Qian, and I.G. Kevrekidis. “coarse” stability and bifurcation analysis using timesteppers: a reaction diffusion example. *Proc. Natl. Acad. Sci.*, 97:9840–9843, 2000.
- [46] A. Varshney and A. Armaou. Optimal operation of GaN thin film epitaxy employing control vector parameterization. *AIChE J.*, submitted, 2004.

- [47] S. Vasantharajan, J. Viswanathan, and L. T. Biegler. Reduced successive quadratic programming implementation for large-scale optimization problems with smaller degrees of freedom. *Comput. Chem. Eng.*, 14:907–915, 1990.
- [48] V. S. Vassiliadis. *Computational Solution of Dynamic Optimization Problems with General Differential-Algebraic Constraints*. PhD thesis, Imperial College, University of London, UK, 1993.
- [49] V. S. Vassiliadis, R. W. H. Sargent, and C. C. Pantelides. Solution of a class of multistage dynamic optimization problems, parts I & II. *Ind. & Eng. Chem. Res.*, 33:2111–2133, 1994.
- [50] J. Wolff, A. G. Papathanasiou, I. G. Kevrekidis, H. H. Rotermund, and G. Ertl. Spatio-temporally addressing surface activity. *Science*, 294:134–137, 2001.

Table 1: NO reduction process parameters

| Parameter | Value | Steady states |
|-----------|-------|------------------------|
| T | 0.25 | $\theta_{ss,s}$ 0.3301 |
| N | 20 | $\theta_{ss,i}$ 0.6803 |
| t_f | 5 | $\theta_{ss,f}$ 0.9896 |
| k_{ss} | 0.45 | |
| α | 1.0 | |
| γ | 0.01 | |

Table 2: Hooke-Jeeves search results

| Model | N_l | M_r | Objective | t^* [s] |
|--------|------------------|-------|-----------|-----------|
| Legacy | — | — | 10.3709 | 129 |
| KMC | 100×100 | 200 | 10.5418 | 674 |
| KMC | 200×200 | 400 | 10.4155 | 4673 |
| KMC | 300×300 | 600 | 10.3973 | 16300 |
| KMC | 400×400 | 800 | 10.3815 | 38469 |
| KMC | 500×500 | 1000 | 10.3811 | 75307 |

* single CPU pentium *IV* at 2.4 *GHz*

Table 3: Implicit Filtering search results

| Model | d_{max} | Scales | Objective | t^* [s] |
|--------|-----------|-------------------------|-----------|-----------|
| Legacy | — | — | 10.3709 | 168 |
| KMC | 0.005 | $2^{-0}, \dots, 2^{-3}$ | 10.5461 | 297 |
| KMC | 0.005 | $2^{-0}, \dots, 2^{-4}$ | 10.7922 | 282 |
| KMC | 0.0005 | $2^{-3}, \dots, 2^{-5}$ | 10.4110 | 3684 |
| KMC | 0.001 | $2^{-0}, \dots, 2^{-4}$ | 10.4129 | 6858 |

* single CPU pentium *IV* at 2.0 *GHz*

Table 4: CO oxidation process parameters

| Parameter | Value | Steady states |
|--------------|-------|----------------------------|
| T | 0.25 | $\theta_{CO,ss,s}$.13944 |
| N | 20 | $\theta_{CO,ss,i}$.67526 |
| t_f | 5 | $\theta_{CO,ss,f}$.97101 |
| k_r | 1.0 | $\theta_{O_2,ss,s}$.63553 |
| α | 1.6 | $\theta_{O_2,ss,i}$.11452 |
| γ | 0.04 | $\theta_{O_2,ss,f}$.00137 |
| β_{ss} | 3.5 | |

Table 5: Hooke Jeeves search results. $T = 0.1$, $t_f = 5$

| Model | N_l | M_r | Passes | Objective | Total t [s] |
|--------|------------------|----------|--------|-----------|-------------|
| Legacy | — | — | 3 | 24.8958 | 3381 |
| KMC | 100×100 | 200 runs | 3 | 25.1487 | 8182 |
| KMC | 300×300 | 600 runs | 2 | 24.9997 | 57482* |

*First search used a 100×100 lattice size KMC realization.

Table 6: Hooke Jeeves search results. $t_f = 5$, KMC with 100×100 lattice, 200 runs average

| Model | Timestep | Objective | Total t [s] |
|-------|----------|-----------|-------------|
| KMC | 0.50 | 25.7498 | 481 |
| KMC | 0.25 | 25.4800 | 899 |
| KMC | 0.10 | 25.2734 | 2603 |
| KMC | 0.10* | 25.2607 | 3100 |

* Second pass at desired timestep.

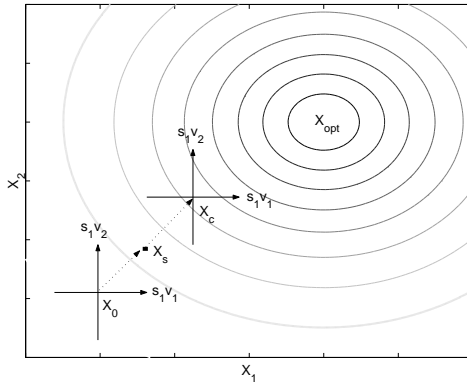


Figure 1: Two-dimensional optimization problem, presenting the steps of one iteration during an optimal search using Hooke-Jeeves algorithm. Darker contour lines denote lower values of objective function.

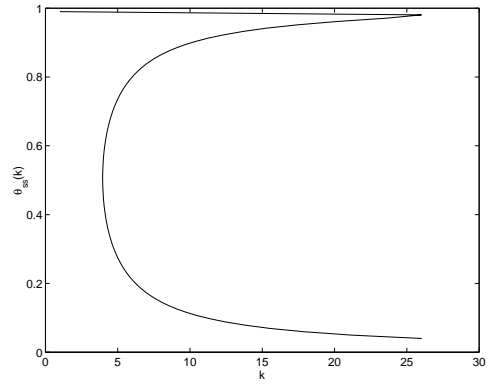


Figure 2: Bifurcation diagram of θ at steady state with respect to k .

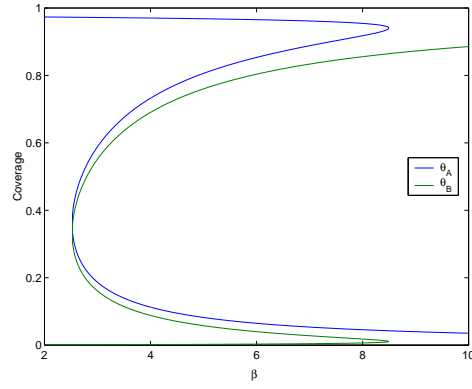


Figure 3: Bifurcation diagram of θ_A and θ_B at steady state with respect to β .

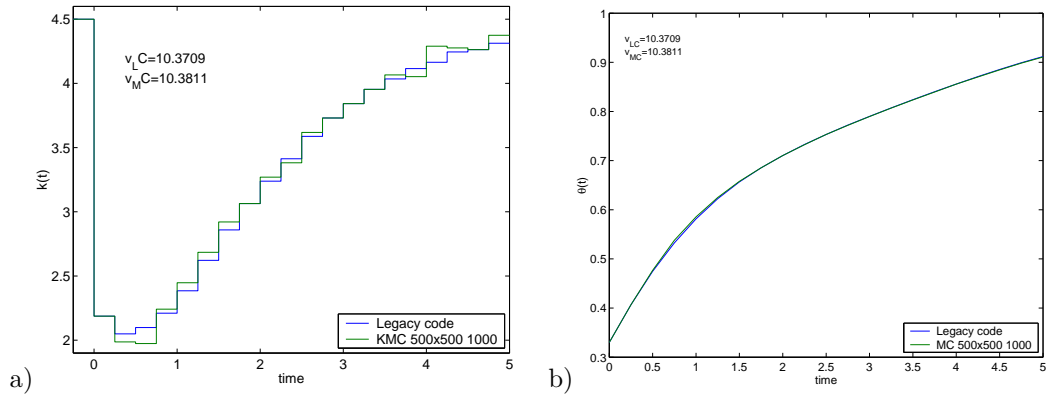


Figure 4: Results using Hooke-Jeeves algorithm through numerical integration of Eq.1 (blue line) and using KMC simulation (green line), a) Optimal temporal profile of process reaction rate k , b) Evolution of NO coverage θ .

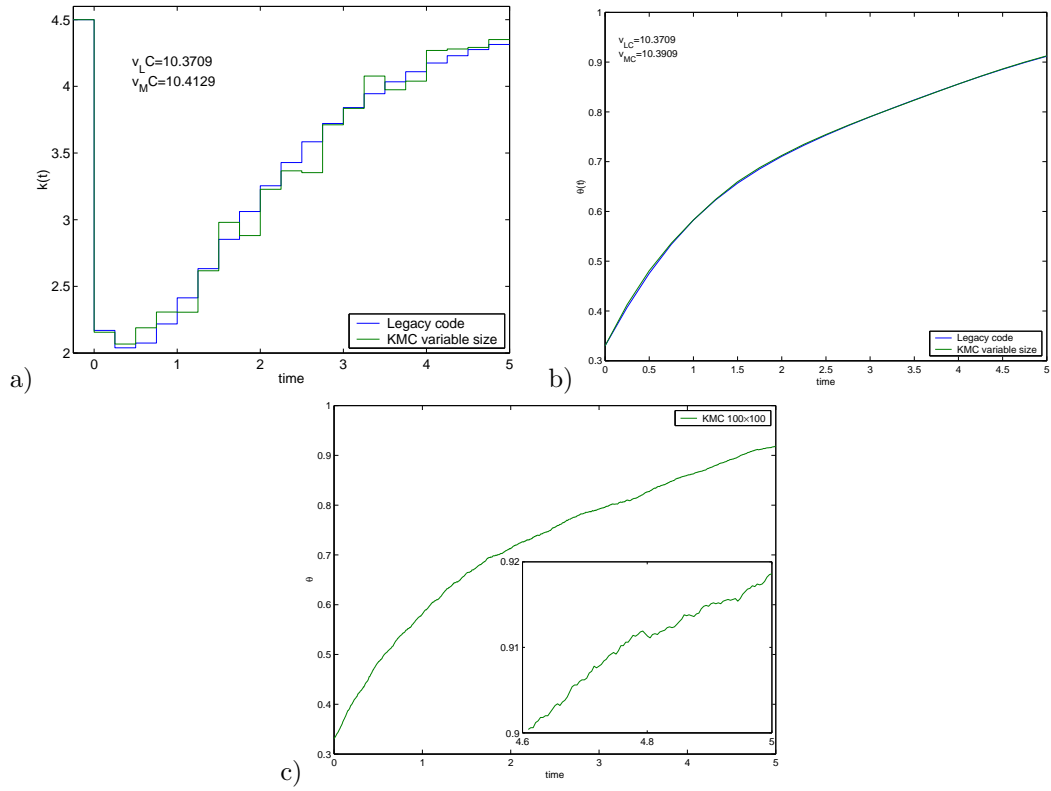


Figure 5: Results using Implicit Filtering algorithm through numerical integration of Eq.1 (blue line) and using KMC simulation (green line), a) Optimal temporal profile of process reaction rate k , b) Evolution of NO coverage θ , c) Evolution of NO coverage θ for a single KMC realization, $N_t = 100 \times 100$, $\delta t = 0.0039$.

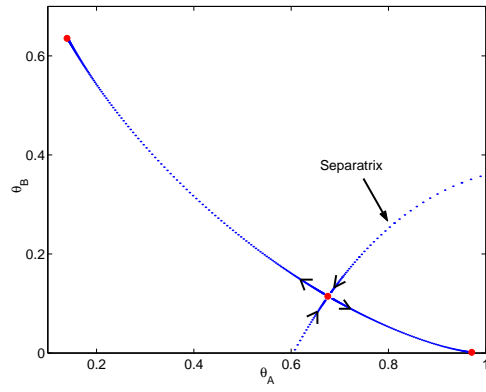


Figure 6: phase portrait of system of Eq.4 presenting the three steady states and the separatrix for $\beta = 3.5$ (process parameter values shown in Table 4).

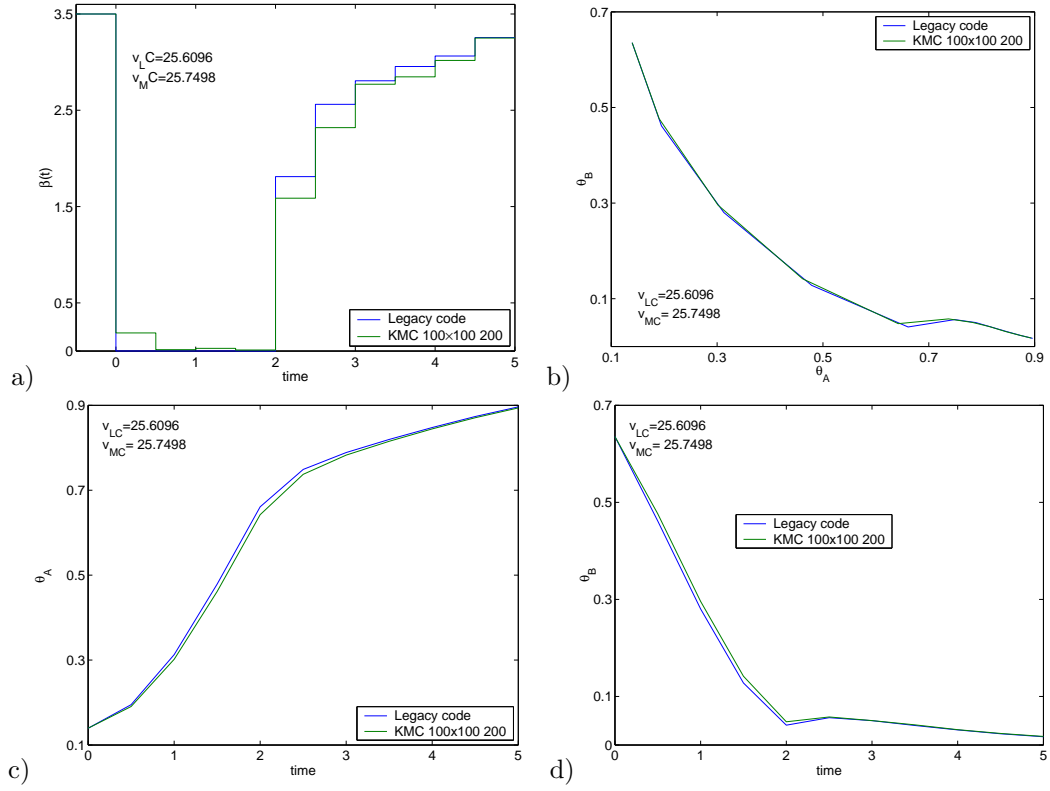


Figure 7: Results of Hooke-Jeeves algorithm through numerical integration of Eq.4 (blue line) and using KMC simulations with 100×100 lattice size and 200 repetitions (green line), a) Optimal temporal profile of O_2 adsorption rate β , b) phase portrait of process evolution, c) evolution of CO coverage θ_A , d) evolution of O_2 coverage θ_B ($t_f = 5$, $N = 10$, $\beta_{ss} = 3.5$).

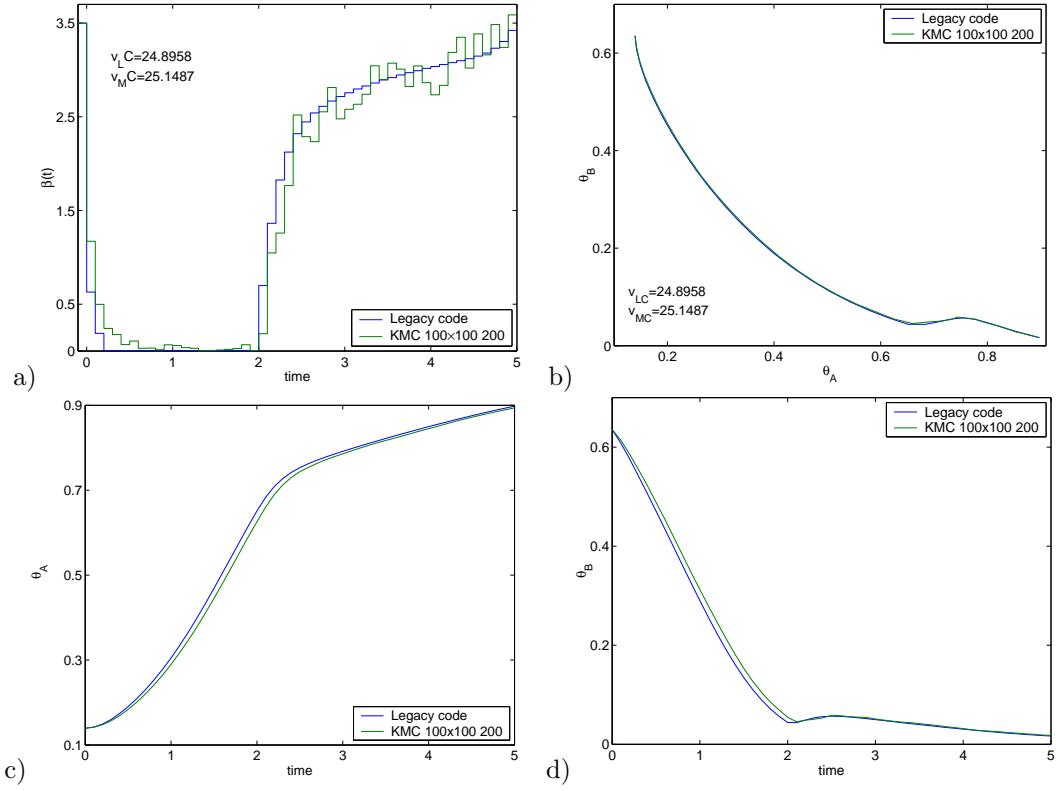


Figure 8: Results of Hooke-Jeeves algorithm through numerical integration of Eq.1 (blue line) and using KMC simulations with 100×100 lattice size and 200 repetitions (green line), a) Optimal temporal profile of O_2 adsorption rate β , b) phase portrait of process evolution, c) evolution of CO coverage θ_A , d) evolution of O_2 coverage θ_B ($t_f = 5$, $N = 50$, $\beta_{ss} = 3.5$).

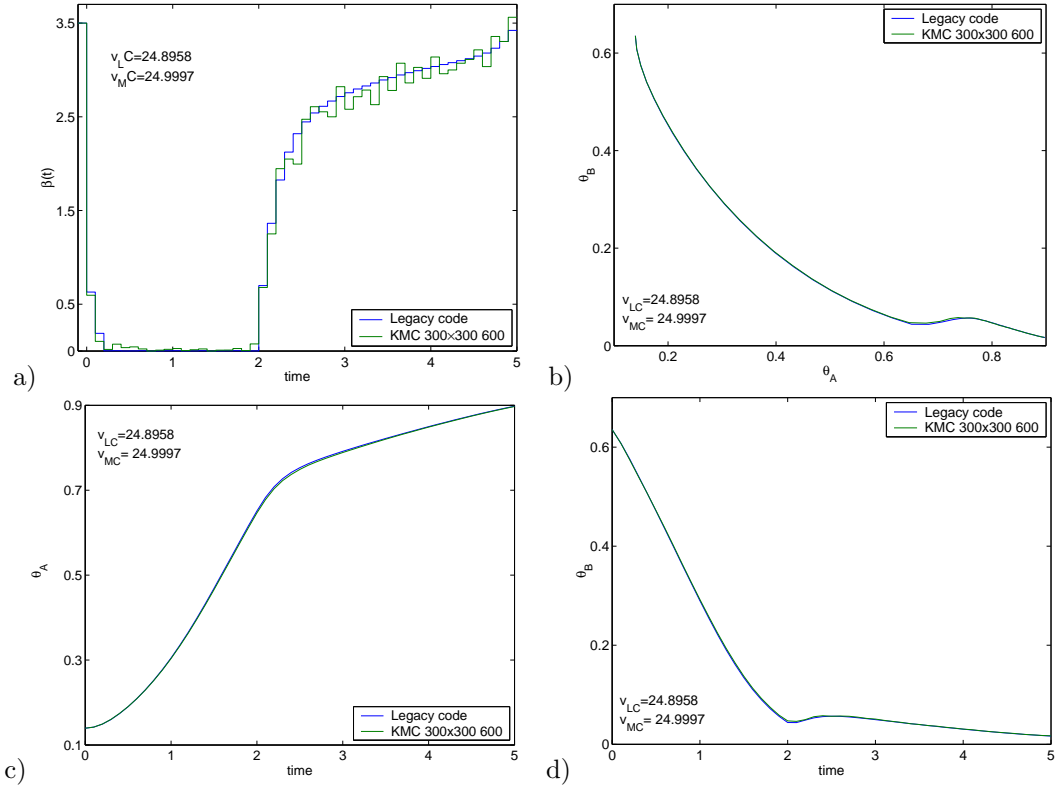


Figure 9: Results of numerical integration of Eq.4 (blue line) and KMC simulations with 300×300 lattice size averaged over 600 runs (green line), a) Optimal temporal profile of O_2 adsorption rate β , identified by Hooke-Jeeves search algorithm, b) phase portrait of process evolution, c) evolution of CO coverage θ_A , d) evolution of O_2 coverage θ_B ($t_f = 5$, $N = 50$, $\beta_{ss} = 3.5$).

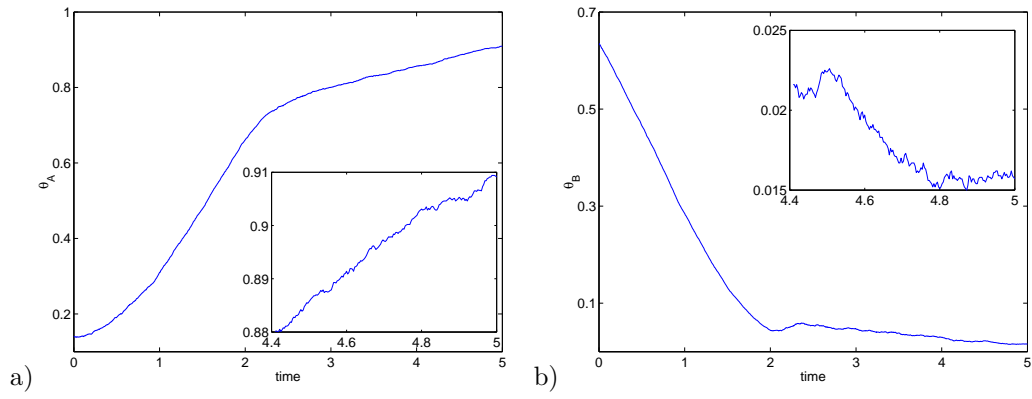


Figure 10: a) evolution of CO coverage θ_A , b) evolution of O_2 coverage θ_B , for a single KMC realization, $N_l = 100 \times 100$, $\delta t = 0.0031$, for the Hooke-Jeeves computed β temporal profile ($\beta_{ss} = 3.5$).

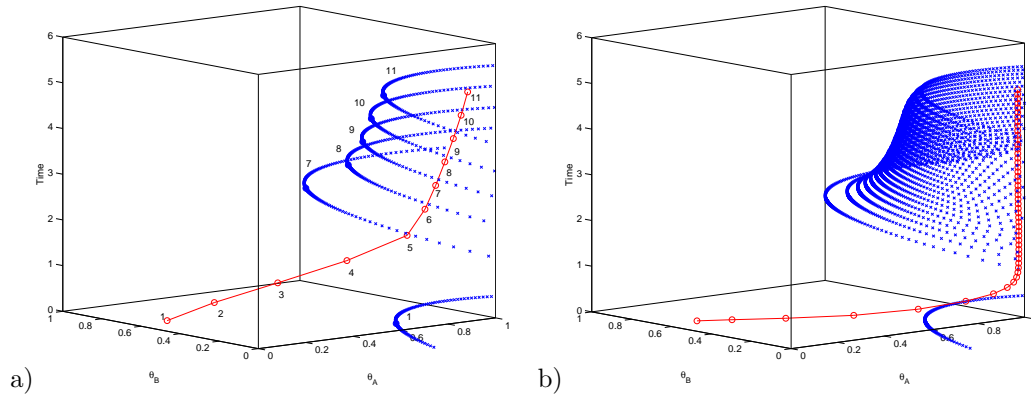


Figure 11: Optimal trajectory for system of Eq.4 (red line), identified by Hook-Jeeves search algorithm, and evolution of separatrix (blue line), a) for $N = 10$, b) FOR $N = 50$, identified by $(t_f = 5, \beta_{ss} = 3.5)$.